A Facile Aqueous Route to Nitrogen-Doped Mesoporous Carbons

Jianan Zhang[a,b,c‡], Yang Song[a,d‡], Maciej Kopeć[a], Jaejun Lee[b], Zongyu Wang[a], Siyuan Liu[b], Jiajun Yan[a], Rui Yuan[a], Tomasz Kowalewski[a], Michael R. Bockstaller[*b] and Krzysztof Matyjaszewski[*a]

[a]Department of Chemistry and [b]Department of Materials Science and Engineering, Carnegie Mellon University, Pittsburgh, PA 15213, United States

[c]School of Chemistry and Chemical Engineering, Anhui University, Hefei 230601, China

[d]Institute of Nuclear and New Energy Technology, Tsinghua University, Beijing 100084, China

Supporting Information Placeholder

ABSTRACT: An aqueous-based approach for the scalable synthesis of nitrogen-doped porous carbons with high specific surface area (SSA) and high nitrogen content is presented. Low molecular weight polyacrylonitrile (PAN) is solubilized in water in the presence of ($ZnCl_2$) that also acts as a volatile porogen during PAN pyrolysis to form mesoporous structures with significantly increased SSA. By templating with commercial SiO_2 nanoparticles, nanocellulose fillers or filter paper, nanocarbons with SSA = 1776, 1366 and 1501 m^2/g, respectively and 10 wt.% N content were prepared. The materials formed by this benign process showed excellent catalytic activity in oxygen reduction reaction (ORR) *via* the four-electron mechanism.

Large specific surface area (SSA), high porosity, chemical inertness and thermal stability make porous carbons ubiquitous materials in applications such as catalysis, water/gas purification, or energy conversion/storage.[1] Nitrogen (N)-doped carbons have attracted particular interest, due to their potential as metal-free electrocatalysts for oxygen reduction reactions (ORR), a key process in fuel cell technology and metal-air batteries.[1-4] Dai *et al.* first demonstrated that N-doped carbons can facilitate ORR *via* the four-electron pathway and perform better than state-of-the-art Pt/C catalysts.[2] This spurred extensive research to establish N-doped carbons for other applications, such as hydrogen evolution reaction (HER),[3] CO_2 reduction[3b] or supercapacitors.[4] Interconnected mesopores enhance mass transport and access to active sites and thus are crucial for efficient ORR electrocatalys..[5]

Porous carbons are typically synthesized by direct carbonization of organic precursors such as polymers or biomass using a variety of chemical or physical activation methods.[1,6,7] Polyacrylonitrile (PAN) is an attractive precursor for N-doped carbons, due to its high nitrogen content and well-established carbonization chemistry. Mesoporous carbons were synthesized from PAN via hard-[4a,8] or soft-templating[4b,9] procedures. However, this approach requires the use of polar organic solvents and multistep surface functionalization or block copolymerization to disperse templates within PAN. [15, 10]

We demonstrate that the addition of $ZnCl_2$ (a volatile electrolyte) enables the effective co-solubilization of PAN within aqueous dispersions of porogenic fillers,such as commercial Ludox SiO_2 colloids or nanocellulose, and the subsequent fabrication of highly porous carbons. $ZnCl_2$ serves the dual role of a solubility enhancing porogen. The dual pore formation mechanism (i.e. concurrent hard templating and electrolyte evaporation) results in nano-and mesoporous microstructures with strongly increased SSA. Infiltration of cellulose filters with aqueous PAN/$ZnCl_2$ solutions yields bulk monolithic N-doped nanocarbon films without binder components. The general approach is illustrated in Scheme 1.

Scheme 1. Procedure for preparation of mesoporous carbons.

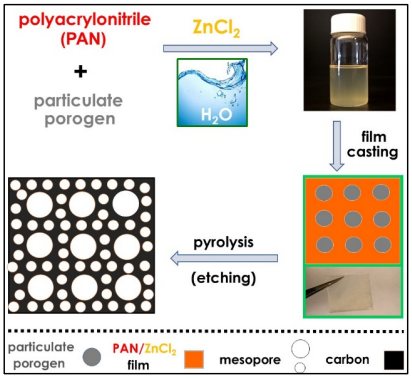

We first demonstrate the versatility of the aqueous route to nitrogen-doped mesoporous carbons from templated PAN solution by using commercial aqueous suspension of SiO_2 NPs (diameter 12.5 ± 1.5 nm, Figure S1). To ensure complete dissolution of PAN in aqueous $ZnCl_2$ (60 wt%) and an operable viscosity of the SiO_2/$ZnCl_2$/PAN suspension, PAN with a degree of polymerization (DP) of 50 and narrow molecular weight distribution (M_w/M_n < 1.20) was used (Figure S2), which was synthesized by initiators for continuous activator regeneration atom transfer radical polymerization (ICAR ATRP) with ppm amounts of copper catalyst[11] or directly in aqueous $ZnCl_2$ solution.[12] Upon freeze drying of SiO_2/$ZnCl_2$/PAN suspensions, hybrid scaffolds were obtained. Subsequent stabilization at 280 °C under air followed by carbonization at 800 °C under N_2 and etching of the SiO_2 template with HF yielded mesoporous carbons.

Commented [KM(1]: This is repeated in the next sentence.

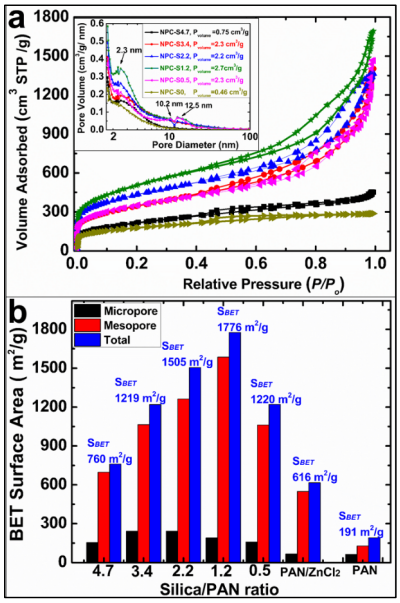

Figure 1. (a) N_2 adsorption and desorption isotherms and (b) contribution of different pore sizes to the total S_{BET} of the as-prepared nanoporous carbons. Inset shows the pore size distribution in materials prepared with different ratios of SiO_2/PAN.

Figure 1a shows Brunauer-Emmet-Teller (BET) N_2 adsorption isotherms for carbons prepared from samples with systematically varied compositions, SiO_2:PAN= 4.7, 3.4, 2.2, 1.2, 0.5 (i.e. with progressively higher PAN concentration, cf. Scheme S1) along with a sample prepared without the addition of colloidal SiO_2 NPs. These materials are identified as NPC-S4.7, NPC-S3.4, NPC-S2.2, NPC-S1.2, NPC-S0.5, and NPC-S0, respectively. All adsorption isotherms are type IV according to IUPAC classification and exhibit distinctive hysteresis loops at relative pressures of 0.6–0.9, indicative of filling and emptying of mesopores by capillary condensation/evaporation. The BET surface areas (S_{BET}) and total pore volumes are listed in Table S1. As can be seen from Figure 1a, even the sample carbonized without the addition of SiO_2 exhibited significant S_{BET} of 616 m^2/g with large contribution from mesopores (S_{meso}=549 m^2/g, Figure 1b and Table S1). The corresponding pore size distribution (PSD, inset in Figure 1a) displayed a small mesopore peak centered at 2.3 nm tailing up to ~8 nm. The high S_{meso} originated from activation by $ZnCl_2$, since PAN (DP50) carbonized without the addition of $ZnCl_2$ had a much lower S_{BET} = 191 m^2/g and no pronounced hysteresis loop in the adsorption isotherm, indicating a predominately microporous material (Figure S3a). Interestingly, $ZnCl_2$ activation did not increase the microporosity, but selectively enhanced the S_{meso} of PAN-derived carbons (Figure S3b and Table S1). The selective formation of mesopores could be due to the low molecular weight PAN matrix that is more conducive to the transport of gaseous electrolyte.[13] $ZnCl_2$ likely promoted dehydration of PAN and aromatization of nitrile groups (Figure S4).[13b] Furthermore, $ZnCl_2$ mixed with PAN decomposed at a temperature lower than pure $ZnCl_2$ and completely volatilized below 550 °C, thus allowing for complete removal of the salt during pyrolysis above 600 °C.[14]

After the addition of SiO_2 particles to the PAN/$ZnCl_2$ solution, the S_{BET} of obtained carbons increased to 1220, 1776 and 1505 m^2/g for samples NPC-S0.5, NPC-S1.2 and NPC-S2.2, respectively, with $ZnCl_2$-induced mesopores accounting for as much as 84-90% of the total SSA (Table S1). This remarkably high S_{meso} originated from a synergistic effect of $ZnCl_2$ activation and SiO_2 templating. Indeed, the mesopore peak centered at 2.3 nm, similar to one observed for NPC-S0, was still visible in PSD of all SiO_2-templated samples. However, the evolution of two new peaks, at 10.2 and 12.5 nm, corresponding to the size of the SiO_2 NPs (12.5±1.5 nm), is clearly visible. Since a broad distribution of mesopores was observed rather than a narrow peak corresponding to 12.5 nm SiO_2 NPs, partial aggregation of NPs during the freeze drying and carbonization processes is possible. Further increase of the SiO_2/PAN ratio resulted in a decrease of S_{BET} of corresponding carbons to 1219 and 760 m^2/g for NPC-S3.4 and NPC-S4.7, respectively. The pores originating from SiO_2 NPs were no longer visible in PSD of NPC-S4.7, resembling that of NPC-S0 (inset in Figure 1a). This is attributed to an insufficient amount of PAN to efficiently encapsulate the SiO_2 NPs(Figure S5).

To evaluate the more general applicability of the co-solubilization approach to all-organic systems, commercial cellulose nanocrystals as well as cellulose filter paper were used as templates to prepare nanoporous carbons.[15] Figure 2 compares the BET N_2 adsorption isotherms and the corresponding PSD (Figure S6) of porous carbons prepared from commercial cellulose nanocrystals (NPC-C) and filter paper (NPC-P) with materials obtained after infiltration with $ZnCl_2$ (NPC-CZ, NPC-PZ) and PAN/$ZnCl_2$ (NPC-PZ, NPC-PAZ), respectively.

Commented [KM(2]: Maybe move some of it to the SI, if necessary.

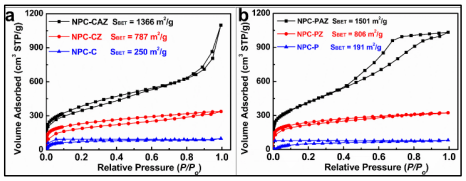

Figure 2. N_2 adsorption isotherms of porous carbons prepared from nanocellulose (a) and cellulose filter paper (b).

$ZnCl_2$ activation enabled the formation of highly porous carbon with S_{BET} of 1366 and 1501 m^2/g for nanocellulose and filter paper templated systems, respectively. In both cases the PSD revealed the formation of mesopores with diameter 2.3 nm that can be attributed to the volatilization of $ZnCl_2$ (Figure S6). The size of mesopores was approximately equal for all studied templates and the PSD was narrower for PAN/$ZnCl_2$ infiltrated systems. Thus, the cumulative effect of $ZnCl_2$ volatilization and PAN carbonization determines the final size of mesopores. The type H3 loop characteristics was observed for both NPC-CAZ and NPC-PAZ and attributed to the fibrous morphology of the template that favors the formation of slit-shaped pores.[16]

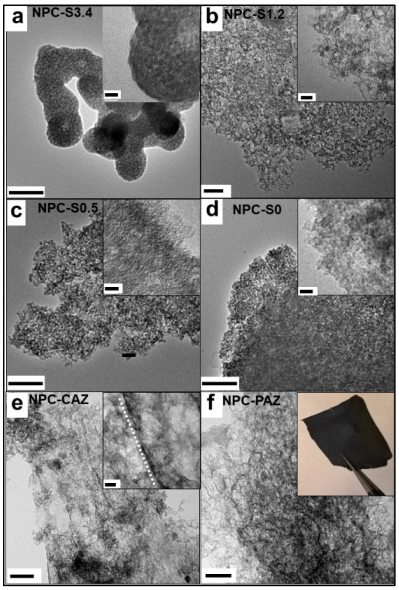

Figure 3. Representative TEM images of porous carbon prepared at SiO_2/PAN ratios of (a) 3.4, (b) 1.2, (c) 0.5, and (d) without the addition of colloidal SiO_2 NPs, templated from cellulose nanocrystals (e) and filter paper (f) after infiltration with PAN/$ZnCl_2$ solution. Inset in (f) shows the optical picture of the corresponding porous carbon film. Scale bars are 200 nm in main figures and 20 nm in insets.

Transmission electron microscopy (TEM) revealed the increase of the density of micropores with SiO_2 content (Figure 3a-d) as well as the more anisotropic pore structure of cellulose-derived NPCs (Figure 3e&f). A comprehensive comparison of the microstructures is shown in Figures S7-S11. Interestingly, carbonization of filter paper infiltrated with PAN/$ZnCl_2$ solution allowed fabrication of free-standing, monolithic NPC films(inset in Figure 3f).

XRD and Raman spectroscopy demonstrated the co-existence of graphitic and disordered morphologies (Figure S12). Elemental composition of the prepared mesoporous carbon (NPC-S1.2) was determined by elemental analysis (combustion method) with the nitrogen content of 10 wt%, consistent with typical values for PAN-derived carbons prepared at this temperature (800 ºC)[4b].

This composition was confirmed by analysis of the X-ray photoelectron spectroscopy (XPS) survey spectrum of NPC-S1.2 (Figure S13). Respective atomic contents of carbon, nitrogen and oxygen were found to be 84.0 %, 9.6% and 4.9%.. Similar nitrogen contents obtained from elemental analysis and XPS indicate the uniformity of nitrogen distribution in the material. The high resolution N1s spectrum (Figure 4a) was deconvoluted to three peaks with the binding energies of 403.3, 399.9, and 398.2 eV, attributed to pyridine oxide-N (N-O), pyrrolic- or pyridonic-N (N-X), and pyridinic-N (N-P), respectively. The ratios of different nitrogen types are 21.7 % (pyridinic-N), 56.7 % (pyridonic- or pyrrolic-N) and 21.6 % (pyridine oxide-N). Furthermore, the full width at half-maximum (fwhm) of the N−P peak was only 1.4 eV. This is significantly less than previously reported values for pyridinic nitrogen in pyrolytic carbons derived from PAN, demonstrating the high degree of uniformity of NPCs.[17]

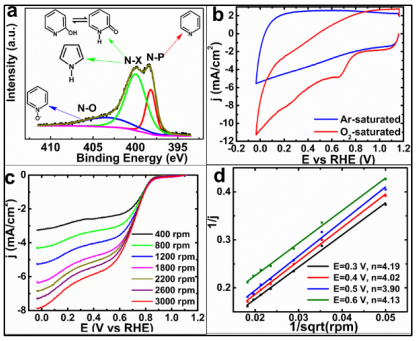

Figure 4. (a) XPS N 1s spectrum of the NPC-S1.2. Electrochemical characterization of NPC-S2.2 as an electrocatalyst for ORR: (b) CV curves recorded N_2-saturated and O_2-saturated 0.1 M KOH electrolyte at a scan rate 100 mV/s; (c) rotating disk electrode study in O_2-saturated 0.1 M KOH electrolyte at a scan rate 10 mV/s; (d) Koutecky-Levich analysis of LSV curves presented in (c).

The electrocatalytic activity of prepared carbons towards ORR was evaluated for the NPC-S2.2 sample in a standard three-electrode setup at room temperature in 0.1 M KOH as the electrolyte. The active material was deposited on a glassy carbon disk and used as the working electrode with a Ag/AgCl reference electrode and graphite counter electrode. Cyclic voltammetry (CV) scans recorded at 100 mV/s showed no redox peak when the electrolyte was continuously purged with argon. In contrast, when the solution was saturated with O_2, a pronounced cathodic peak appeared in the CV scan (Figure 4b). Linear sweep voltammograms (LSV) were recorded using a rotating disk electrode (RDE) at different rotation speeds. As can be seen from the polarization curves in Figure 4c, the onset potential of NPC-S2.2 based electrode was ~0.9 V vs RHE, comparable with that of commercial Pt/C catalysts. The limiting current gradually increased with rotation speed. Since ORR can proceed *via* either two- or four- electron transfer mechanism, Koutecky–Levich analysis was performed to determine the number of transferred electrons (n_e). The linear relationship between the current density (j^{-1}), as a function of a square root of the rotation speed ($\omega^{-1/2}$) in the potential range of 0.3-0.6 V vs RHE can be inferred from the Koutecky-Levich plots (Figure 4d). The number of electrons (n_e) transferred in the process determined by the Koutecky-Levich equations ranged between 3.90 and 4.19. This suggests that the ORR process occurred via the four-electron pathway, as expected based on the structural characteristics of this N-doped mesoporous carbon.[1b]

To conclude, we have developed a facile, benign and scalable aqueous-based method for synthesis of mesoporous N-doped carbons that can be applied to both inorganic and all-organic templating. Application of $ZnCl_2$ as solubility enhancing porogen enables the solubilization of PAN and dispersion of porogenic particle fillers in water and significantly enhances the surface area as compared to regular templated systems. The resulting materials exhibited high nitrogen content and showed excellent catalytic activity toward ORR *via* the four-electron mechanism. This method opens new possibilities for preparation of porous carbons under environmentally-friendly conditions.

ASSOCIATED CONTENT

Supporting Information

The Supporting Information is available free of charge on the ACS Publications website. Experimental details, characterization, supplementary discussion, Table S1, Scheme S1, and Figures S1−S12 (PDF)

AUTHOR INFORMATION

Corresponding Author

*bockstaller@cmu.edu
*km3b@andrew.cmu.edu

ORCID

Michael R. Bockstaller: 0000-0001-9046-9539
Krzysztof Matyjaszewski: 0000-0003-1960-3402

Author Contributions

‡These authors contributed equally.

Notes

The authors declare no competing financial interests.

ACKNOWLEDGMENT

Support from the NSF (via grants DMR 1501324 and CMMI 1663305) is acknowledged. J.Z. acknowledges a scholarship from the China Scholarship Council (CSC). M.K. thanks Polish Ministry of Science and Higher Education ("Mobilnosc Plus" grant no. 1055/MOB/2013/0) for financial support. J.Z. and M.R.B. further acknowledge support by the Scott Energy Institute at Carnegie Mellon University.

REFERENCES

1. a) Zhang, S.; Kang, P.; Ubnoske, S.; Brennaman, M. K.; Song, N.; House, R. L.; Glass, J. T.; Meyer, T. J. *J Am Chem Soc* **2014**, *136*, 7845-7848; b) Dai, L.; Xue, Y.; Qu, L.; Choi, H.-J.; Baek, J.-B. *Chem. Rev.* **2015**, *115*, 4823-4892; c) Liang, H.-W.; Brüller, S.; Dong, R.; Zhang, J.; Feng, X.; Müllen, K. *Nat. Commun.* **2015**, *6*; d) Marsh, H.; Rodríguez-Reinoso, F. In *Activated Carbon*; Elsevier Science Ltd: Oxford, 2006; e) Li, W.; Liu, J.; Zhao, D. *Nat. Rev. Mater.* **2016**, *1*, 16023; f) Liang, C.; Li, Z.; Dai, S. *Angew. Chem. Int. Ed.* **2008**, *47*, 3696-3717.
2. Gong, K.; Du, F.; Xia, Z.; Durstock, M.; Dai, L. *Science* **2009**, *323*, 760-764.
3. a) Zheng, G.; Lee, S. W.; Liang, Z.; Lee, H. W.; Yan, K.; Yao, H.; Wang, H.; Li, W.; Chu, S.; Cui, Y. *Nat Nanotechnol* **2014**, *9*, 618-623; b) Hu, C.; Dai, L. *Angew. Chem. Int. Ed. Engl.* **2016**, *55*, 11736-11758.
4. a) Yang, X.; Wu, D.; Chen, X.; Fu, R. *J. Phys. Chem. C* **2010**, *114*, 8581-8586; b) Zhong, M.; Kim, E. K.; McGann, J. P.; Chun, S.-E.; Whitacre, J. F.; Jaroniec, M.; Matyjaszewski, K.; Kowalewski, T. *J. Am. Chem. Soc.* **2012**, *134*, 14846-14857; c) Lin, T.; Chen, I. W.; Liu, F.; Yang, C.; Bi, H.; Xu, F.; Huang, F. *Science* **2015**, *350*, 1508-1513.
5. a) Guo, D.; Shibuya, R.; Akiba, C.; Saji, S.; Kondo, T.; Nakamura, J. *Science* **2016**, *351*, 361-365; b) Wei, W.; Liang, H.; Parvez, K.; Zhuang, X.; Feng, X.; Müllen, K. *Angew. Chem.* **2014**, *126*, 1596-1600; c) Chang, H.; Joo, S. H.; Pak, C. *J. Mater. Chem.* **2007**, *17*, 3078-3088.
6. Wu, X.; Shi, Z.; Tjandra, R.; Cousins, A. J.; Sy, S.; Yu, A.; Berry, R. M.; Tam, K. C. *J. Mater. Chem. A* **2015**, *3*, 23768-23777.
7. Pang, Q.; Tang, J.; Huang, H.; Liang, X.; Hart, C.; Tam, K. C.; Nazar, L. F. *Adv. Mater.* **2015**, *27*, 6021-6028.
8. a) Cao, L.; Kruk, M. *Polymer* **2015**, *72*, 356-360; b) Kruk, M.; Dufour, B.; Celer, E. B.; Kowalewski, T.; Jaroniec, M.; Matyjaszewski, K. *J. Phys. Chem. B* **2005**, *109*, 9216-9225; c) Jang, J.; Lim, B.; Choi, M. *Chem. Commun.* **2005**, 4214-4216; d) Tang, C.; Bombalski, L.; Kruk, M.; Jaroniec, M.; Matyjaszewski, K.; Kowalewski, T. *Adv. Mater.* **2008**, *20*, 1516-1522; e) Kruk, M.; Kohlhaas, K. M.; Dufour, B.; Celer, E. B.; Jaroniec, M.; Matyjaszewski, K.; Ruoff, R. S.; Kowalewski, T. *Microporous Mesoporous Mater.* **2007**, *102*, 178-187; f) Lu, A.; Kiefer, A.; Schmidt, W.; Schüth, F. *Chem. Mater.* **2004**, *16*, 100-103.
9. Zhong, M.; Jiang, S.; Tang, Y.; Gottlieb, E.; Kim, E. K.; Star, A.; Matyjaszewski, K.; Kowalewski, T. *Chem. Sci.* **2014**, *5*, 3315-3319.
10. Liang, J.; Zheng, Y.; Chen, J.; Liu, J.; Hulicova‐Jurcakova, D.; Jaroniec, M.; Qiao, S. Z. *Angew. Chem.* **2012**, *124*, 3958-3962.
11. a) Matyjaszewski, K.; Tsarevsky, N. V. *J. Am. Chem. Soc.* **2014**, *136*, 6513-6533; b) Lamson, M.; Kopeć, M.; Ding, H.; Zhong, M.; Matyjaszewski, K. *J. Polym. Sci., Part A: Polym. Chem.* **2016**, *54*, 1961-1968; c) Matyjaszewski, K.; Mu Jo, S.; Paik, H.-j.; Gaynor, S. G. *Macromolecules* **1997**, *30*, 6398-6400; d) Zhong, M.; Natesakhawat, S.; Baltrus, J. P.; Luebke, D.; Nulwala, H.; Matyjaszewski, K.; Kowalewski, T. *Chem. Commun.* **2012**, *48*, 11516-11518; e) Matyjaszewski, K.; Xia, J. *Chem. Rev.* **2001**, *101*, 2921-2990; f) Matyjaszewski, K. *Macromolecules* **2012**, *45*, 4015-4039; g) Ribelli, T. G.; Konkolewicz, D.; Pan, X.; Matyjaszewski, K. *Macromolecules* **2014**, *47*, 6316-6321.
12. Kopeć, M.; Krys, P.; Yuan, R.; Matyjaszewski, K. *Macromolecules* **2016**, *49*, 5877-5883.
13. a) Rodriguez-Reinoso, F.; Molina-Sabio, M. *Carbon* **1992**, *30*, 1111-1118; b) Yue, Z.; Mangun, C. L.; Economy, J. *Carbon* **2002**, *40*, 1181-1191.
14. Kim, C.; Ngoc, B. T. N.; Yang, K. S.; Kojima, M.; Kim, Y. A.; Kim, Y. J.; Endo, M.; Yang, S. C. *Adv. Mater.* **2007**, *19*, 2341-2346.
15. a) Dutta, S.; Bhaumik, A.; Wu, K. C.-W. *Energy Environ. Sci.* **2014**, *7*, 3574-3592; b) Yang, W.; Zhai, Y.; Yue, X.; Wang, Y.; Jia, J. *Chem. Commun.* **2014**, *50*, 11151-11153; c) De, S.; Balu, A. M.; van der Waal, J. C.; Luque, R. *ChemCatChem* **2015**, *7*, 1608-1629.
16. Shopsowitz, K. E.; Hamad, W. Y.; MacLachlan, M. J. *Angew. Chem. Int. Ed.* **2011**, *50*, 10991-10995.
17. Pels, J.; Kapteijn, F.; Moulijn, J.; Zhu, Q.; Thomas, K. *Carbon* **1995**, *33*, 1641-1653.

Insert Table of Contents artwork here